Graphical Abstract

A computationally efficient hybrid formulation for viscoelastic-viscoplastic polymer solids and structures under large numbers of loading cycles

Issam Doghri, Darith Anthony Hun[a,b], Mohamed Haddad[b], Issam Doghri[b,⋆],
Michael Lackner[c], Zoltan Major[c], Leonhard Doppelbauer[c,d],
Sara Haouala[e]

Highlights

A computationally efficient hybrid formulation for viscoelastic-viscoplastic polymer solids and structures under large numbers of loading cycles

Issam Doghri, Darith Anthony Hun[a,b], Mohamed Haddad[b], Issam Doghri[b,⋆],
Michael Lackner[c], Zoltan Major[c], Leonhard Doppelbauer[c,d],
Sara Haouala[e]

- Multi-scale simulation strategy for viscoelastic-viscoplastic polymers under large numbers of cycles
- Hybrid method combining Laplace-Carson transform and it inversion with viscoelastic-viscoplastic time-homogenization method

A computationally efficient hybrid formulation for viscoelastic-viscoplastic polymer solids and structures under large numbers of loading cycles

Issam Doghri[1,], Darith Anthony Hun[a,b], Mohamed Haddad[b], Issam Doghri[b,⋆], Michael Lackner[c], Zoltan Major[c], Leonhard Doppelbauer[c,d], Sara Haouala[e]

[a] *Computational & Multiscale Mechanics of Materials, ULiège, Liège, 4000, Belgium*

[b] *Institute of Mechanics, Materials and Civil Engineering, UCLouvain, Louvain-La-Neuve, 1348, Belgium*

[c] *Institute of Polymer Product Engineering, Johannes Kepler University , Linz, 4040, Austria*

[d] *Institute of Technical Mechanics, Johannes Kepler University , Linz, 4040, Austria*

[e] *Holtec Europe SL, Plaza de Carlos Trias Betrán, Linz, 4040, Madrid*

Abstract

An original modeling and computational procedure is proposed for thermoplastic polymer solids and structures subjected to large numbers of loading cycles. Since the behaviour remains dissipative and a direct numerical simulation is extremely prohibitive, an efficient hybrid approach with two main pillars is developed. First, a computational method in linear viscoelasticity based on Laplace-Carson transform and its numerical inversion is validated. Next, the time histories of the total strain components thus obtained are given as input to a time homogenization formulation in coupled viscoelasticity-viscoplasticity. To investigate the accuracy and the efficiency of the hybrid method, a numerical study is provided on a 3D lattice polyurethane (TPU) polymer material, where the parameters are identified experimentally. The evaluation of the hybrid method is based on strain, stress and an energy measure against a full reference solution. The time gain factor increases with the number of cycles. A prediction is provided for one milion cycles. The proposed framework focus a basis for high cycle fatigue studies of polymer solid and structures.

Keywords: hybrid computational method, viscoelastic-viscoplastic polymers, low cost simulation, large number of cycles

1. Introduction

Polymers are present in all sectors of industry. Their intrinsic properties and the modern technologies associated with their processing are the key to solve many of today's challenges. The constant improvement of manufacturing techniques and the advances made in materials

⋆Corresponding author.
Email address: issam.doghri@uclouvain.be (Issam Doghri)

are synchronized with the updating of simulation models and methods, from the manufacturing process phase Bahloul et al. (2021), Bahloul et al. (2023) to the identification of macroscopic properties of interest Wu et al. (2020), Magri et al. (2021), allowing multi-scale inference of extremely interesting properties, see Figure. 1. It is known that thermoplastic polymers dissipate energy, even for large numbers of cycles, as shown in Wang et al. (2023), Mortazavian and Fatemi (2017), Desmorat et al. (2007), therefore classical high cycle fatigue approaches based on linear elasticity are not applicable and need an overhaul.

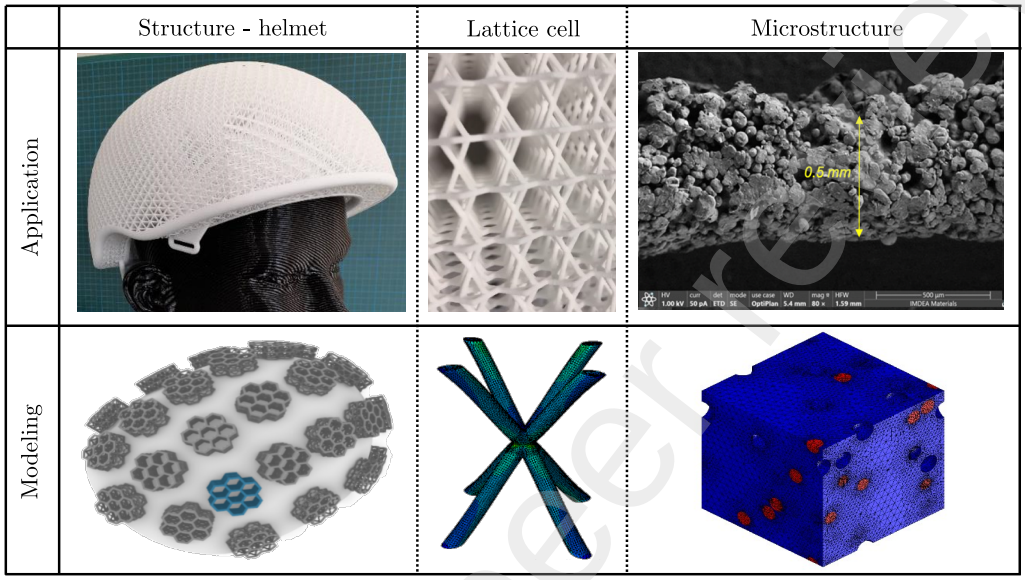

Figure 1: Application and modeling of TPU material

In this article, structures based on TPU polymer printed by selective laser sintering (SLS) technology are subjected to cyclic loadings which, when repeated over a period of time, erode the initial behavior. From an experimental point of view, the associated predictions require costly tests responding to particular constraints, such as limited loading conditions and geometries. Numerical simulations allow us to overcome these constraints. However the numerical cost associated with the complexity of the problem renders the resolution extremly prohibitive. Prediction via the solution of a multi-scale problem, including long-term effects via cyclic loading, structures with complex geometries and non-linear material behavior of the material, represents a formidable challenge.

To address this issue, it is necessary to define a certain framework with two key choices. The first is based on the selection of material model. The literature proposes several models appropriate for mechanical properties of polymers, such as : viscoelastic (VE) Bird and Carreau (1968), Shaw and MacKnight (2018), elastoviscoplastic (EVP) Van Dommelen et al. (2003), Uchida and Tada (2013), Johnsen et al. (2019), and more generally viscoelastic-viscoplastic (VEVP) Hasan and Boyce (1995), Frank and Brockman (2001), Miled et al. (2011). The second choice concerns a computational method for simulating problems subject to cyclic loadings. In the literature, multiple independent numerical methods have been developed Hughes and Stewart (1996), Bottasso (2002), Gravouil and Combescure (2001). For large numbers of cyclic loadings, time-homogenization methods are particularly effective and adapted to polymers because different material models can be used : VE Cognard and

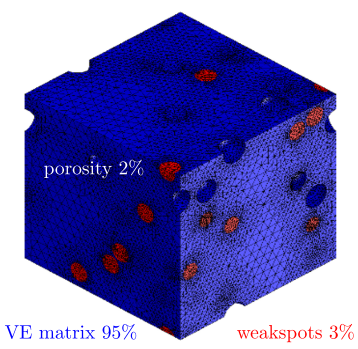

(a) RVE modeling

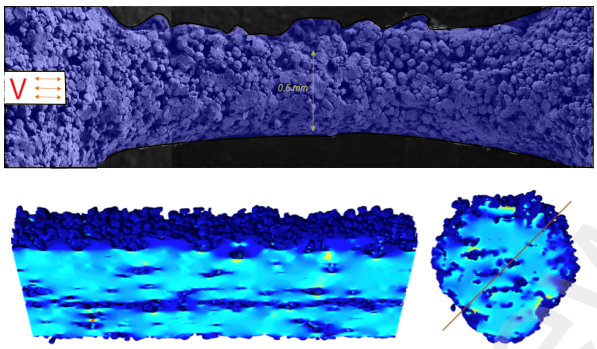

(b) tomography cut of SLS manufacturing material

Figure 2: RVE modeling motivation

Ladevèze (1993), Hun et al. (2023), EVP Guennouni (1988), Oskay and Fish (2004) or VEVP Heczko and Kottner (2018), Haouala and Doghri (2015).

These two key choices are the foundation for predicting the fatigue behavior of a polymer structure subjected to cyclic loadings. The literature proposes two main families of models: coupled models, which have the advantage of being more accurate Balieu et al. (2013), Zaïri et al. (2008), however, in terms of computation time the problem is restricted to a limited number of cycles. On the other side uncoupled models are particularly suitable for large numbers of cycles, based on various fatigue criteria : strain Raphael et al. (2019), stress Kujawski and Ellyin (1995), Mallick and Zhou (2004), energy Tao and Xia (2007), Meneghetti et al. (2014), Santharam et al. (2020) or damage based Meraghni et al. (2011), Krairi and Doghri (2014) and compared/identified with experimental fatigue tests Launay et al. (2013), Jegou et al. (2013). The application of these different failure criteria to anticipate structural fatigue therefore relies on the accuracy of numerical methods to reproduce solutions with a low computational cost. In this work, we investigate this crucial issue. High cycle fatigue simulations will be treated in future work.

The diversity of all these different methods has many advantages, but the difficulty resides in combining them for an effective solution to a structural problem.

To overcome this issue, a multi-scale strategy in space and time is proposed, as illustrated in Fig. 2a. Inspired by the work of Krairi et al. (2016) based on a certain description of the microstructure, the high-cycle fatigue of thermoplastic polymer structures can be described at the micromechanical level by assuming that each representative volume element (RVE) consists of a VE matrix containing small volume fractions of pores (2%) and VEVP weakspots (3%). In the case of SLS-printed polymers, micro-tomographic images corroborate this choice of modeling experimentally (see Fig. 2b). The VE matrix is associated with perfectly sintered material, the pores are manufacturing defects representing infinitesimal spaces between grains and the weakspots an intermediate state. Under the assumptions of large number of cycles and small strains, the idea of this work is therefore to postulate that the structure globally follows a VE deformation throughout the cyclic loading and that the plasticity leading to the weakening of the structure occurs on a microscopic scale in certain local regions, affecting marginally the response of the structure. For the computational point a view, a classical VEVP full-field simulation is not applicable. The idea is to compute the VEVP solution only on regions sensitive to plastification which generate cycle after cycle the weakness of the entire structure.

In order to validate the proposed strategy (see Fig.3), it is crucial to address two significant problems. The first, at the macroscopic scale, involves proposing a method for efficiently solving a structural VE problem under large numbers of cycles. Once the strain history has been obtained at each Gauss point, the next step is to solve a second problem combining this strain history with a time homogenization method Haouala and Doghri (2015) at microscale. This step computes the associated VEVP stress, taking into account microstructure (VE matrix, pores and weakspots) behavior by inferring the VEVP homogenized properties. As the first problem was treated in a previous work Hun et al. (2023), we focus here on the second problem, namely the study aimed to obtaining the deformation/stress (VE/VEVP) solutions via a so-called hybrid method. The homogeneous polymer VEVP properties are identified on experimental tests. A reference solution is obtained by the full calculation of the structure using the VEVP homogeneous properties. The hybrid method needs two sets of properties, VE to access the structural strain history and VEVP to the local stress history using time homogenization. The VE properties are defined as the VE part of the experimentally-based VEVP model, and the VEVP part as the VEVP homogenized model. The link between the two computational methods is based on a hypothesis, assuming that the strain histories between the VE and the VEVP are the same.

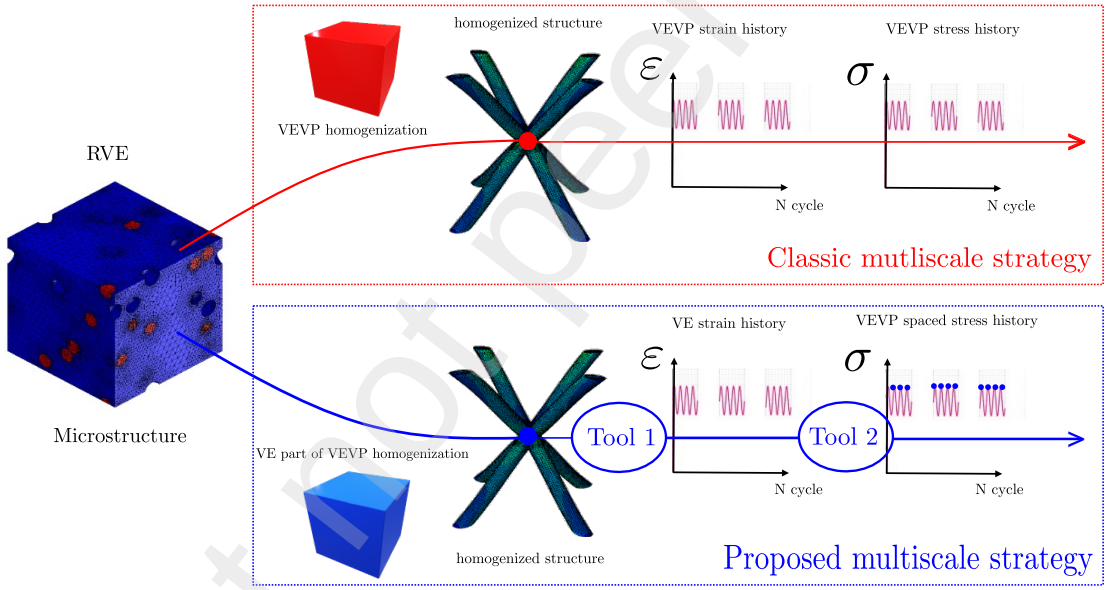

Figure 3: Multiscale strategies

Section 2 summarizes the two methods used : the first is a computational method solving the VE structure problem subjected to large numbers of cycles and the second is a time-homogenization method for VEVP material. Section 3 is dedicated to the identification of polymer properties printed by the SLS process. Section 4 concerns the application of the hybrid method and the validation of the hypothesis linking the two methods. Then, an investigation based on some quantities of interest : strain, stress and an energy measure is provided and compared at several points of the structure with the reference solution, limited computationally to N = 100 cycles. In Section 5, the hybrid method is applied for N = 1 million cycles.

2. Computational framework

The computational framework for polymer solids and structures under large numbers of cycles is based on two pillars which are linked together. The first is Laplace-Carson transform (LCT) followed by LCT inversion proposed in Hun et al. (2023) for VE structures. The second pillar is the time homogenization method proposed in Haouala and Doghri (2015) introduced and motivated for VEVP material. The assumption linking the two pillars is that the total strain histories for VE and VEVP problems are nearly the same. This assumption will be validated in the numerical study in Section 4.

2.1. VE structural problem

2.1.1. General problem

For the mechanical structure problem under the assumption of a quasi-static problem, without ageing, under small perturbations and in linear viscoelasticity, the evolution equations in time t are written as follows:

- Field equations :

$$\mathcal{P}(t): \begin{cases} \boldsymbol{\nabla}.\boldsymbol{\sigma}(\mathbf{x},t) + \rho \boldsymbol{F}(\mathbf{x},t) = 0, \\ \boldsymbol{\varepsilon}(\mathbf{x},t) = \dfrac{1}{2}\Big(\boldsymbol{\nabla}(u(\mathbf{x},t)) + \boldsymbol{\nabla}^T(\mathbf{u}(\mathbf{x},t))\Big), \\ \boldsymbol{\sigma}(\mathbf{x},t) = \displaystyle\int_{-\infty}^{t} \mathbb{C}(\mathbf{x},t-\tau) : \dot{\varepsilon}(\mathbf{x},\tau) d\tau, \end{cases} \tag{1}$$

where $\mathbb{C}(t)$ is the fourth-order isotropic relaxation tensor :

$$\mathbb{C}(t) = 2G(t)\mathbb{I}^{\text{dev}} + 3K(t)\mathbb{I}^{\text{vol}}, \tag{2}$$

the set $(\mathbb{I}^{\text{dev}}, \mathbb{I}^{\text{vol}})$ are respectively the fourth-order deviatoric and volumetric projection tensors and (G, K) are the shear and bulk relaxation moduli expressed here as Prony series :

$$G(t) = G_\infty + \sum_{i=1}^{I} G_i e^{-t/g_i}, \tag{3}$$

$$K(t) = K_\infty + \sum_{j=1}^{J} K_j e^{-t/k_j}. \tag{4}$$

Here (G_∞, K_∞) is the set of long-term moduli, (g_i, k_j) the set of relaxation times, and (G_i, K_j) the set of weights for the shear and bulk moduli.

- Boundary conditions :

$$\mathcal{B}(t): \begin{cases} \partial\Omega_u \cap \partial\Omega_T = \varnothing,\ \partial\Omega_u \cup \partial\Omega_T = \partial\Omega, \\ u_i(\mathbf{x},t) = u_i^d(\mathbf{x},t), \text{ on } \partial\Omega_u, \\ T_i(\mathbf{x},t) = T_i^d(\mathbf{x},t), \text{ on } \partial\Omega_T, \end{cases} \tag{5}$$

where $\partial\Omega_u$ and $\partial\Omega_T$ are respectively the regions where the boundary conditions in displacement u_i^d and the stress vector T_i^d are applied.

2.1.2. Computational method

In order to accelerate the computational time to access to the structural solution, Hun et al. (2023) propose a methodology adapted to solve VE problem under large numbers of cycles. The steps of this work are summarized here :

(1) The mechanical time problem $\{\mathcal{P}(t), \mathcal{B}(t)\}$ (see Eqs.(1) and (5)) is firstly transformed via the LCT in the Laplace-Carson domain defined as :

$$\mathcal{L}_p\{f(t)\} = f^*(p) = p\int_0^\infty f(t)e^{-pt}dt \tag{6}$$

into a linear elastic problem in the L-C domain, see Correspondence principle Mandel (1966/re-edited 1994, J. Gabay.) ,Findley et al. (1989), such as :

- Field equations :

$$\mathcal{P}^\star(p) : \begin{cases} \boldsymbol{\nabla}.\boldsymbol{\sigma}^\star(\mathbf{x},p) + \rho\boldsymbol{F}^\star(\mathbf{x},p) = 0, \\ \boldsymbol{\varepsilon}^\star(\mathbf{x},p) = \dfrac{1}{2}\Big(\boldsymbol{\nabla}(u^\star(\mathbf{x},p)) + \boldsymbol{\nabla}^T(\mathbf{u}^\star(\mathbf{x},p))\Big), \\ \boldsymbol{\sigma}^\star(\mathbf{x},p) = \mathbb{C}^\star(\mathbf{x},p) : \boldsymbol{\varepsilon}^\star(\mathbf{x},p), \end{cases} \tag{7}$$

- Boundary conditions :

$$\mathcal{B}^\star(p) : \begin{cases} \partial\Omega_u \cap \partial\Omega_T = \varnothing,\ \partial\Omega_u \cup \partial\Omega_T = \partial\Omega, \\ u_i^\star(\mathbf{x},p) = u_i^{d\star}(\mathbf{x},p),\ \text{on } \partial\Omega_u, \\ T_i^\star(\mathbf{x},p) = T_i^{d\star}(\mathbf{x},p),\ \text{on } \partial\Omega_T, \end{cases} \tag{8}$$

(2) The boundary conditions ($b_i^d = u_i^d$ or $b_i^d = T_i^d$) are split as follows :

$$b_i^d(\mathbf{x},t) = \widetilde{b}_i^d(\mathbf{x},t) + \widehat{b}_i^d(\mathbf{x},t). \tag{9}$$

This decomposition of the loading signal is used to apply the superposition principle to cumulate the transient response due to the $\widehat{b}_i^d$ function expressed as :

$$\widehat{b}_i^d(t) = \widehat{A}_i(1 - e^{-t/\widehat{\theta}_i}), \tag{10}$$

and the periodic response according to the sinus loading $\widetilde{b}_i^d$ such as :

$$\widetilde{b}_i^d(t) = \widetilde{A}_i \sin(\widetilde{\omega}_i t + \widetilde{\phi}_i), \tag{11}$$

(3) Each subproblem (associated to transient/periodic boundary conditions) needs a particular LCT inversion treatment to recover the solution in time :

- Transient subproblem will use the Schapery LCT inversion (see Sec. 2.1.3),
- Periodic subproblem will use the LCT inversion method based on the sinus basis decomposition (see Sec.2.1.4).

The methodology is depicted in Fig. 4. The numerical implementation details and the excellent accuracy of this method are reported in Hun et al. (2023).

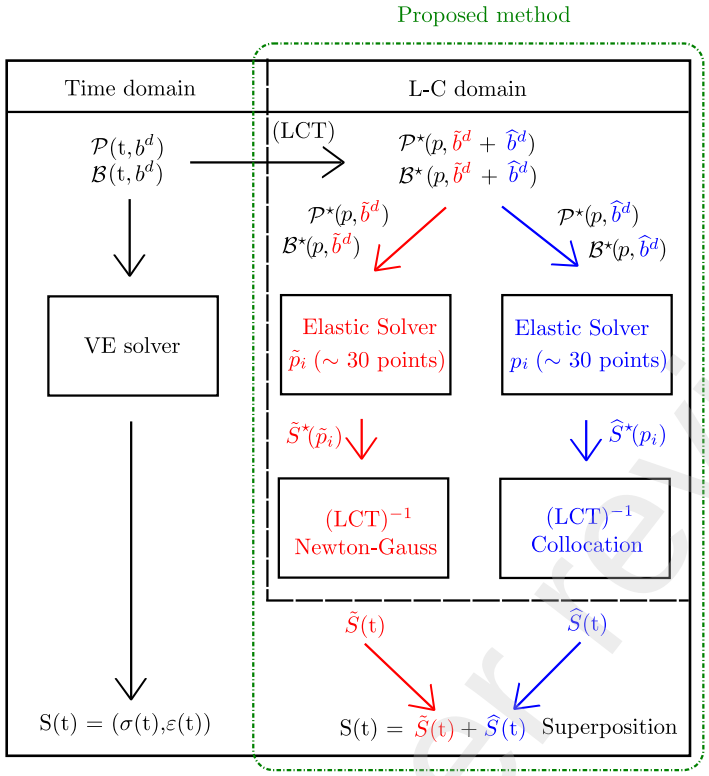

Figure 4: FE simulation strategy of VE structure under cyclic (displacement $b_i^d = u_i^d$ or force $b_i^d = T_i^d$) loading. Left : direct time domain computation to obtain reference solution. Right : proposed procedure in L-C domain followed by split numerical inversion for LCT.

2.1.3. Schapery's collocation method

The collocation method proposed by Schapery (1965) for numerical LCT inversion is still often used in VE mechanical problems. In this framework the author defined the solution f of the problem in time t as a series of exponentials such that :

$$f(t) = A + Bt + \sum_{k=1}^{N} b_k(1 - e^{-t/\theta_k}), \tag{12}$$

This decomposition is parameterized by the set (b_k,θ_k), A and B are shift parameters. This decomposition is adapted to represent both the classical phenomena of creep ($\theta_k < 0$) and relaxation ($\theta_k > 0$) related to a VE behavior.
This decomposition in time of the f solution has its analogous form $f^\star$ in the L-C domain by successive transformation of each term such that :

$$f^\star(p) = A + \frac{B}{p} + \sum_{k=1}^{N} b_k \frac{1}{1 + p\theta_k}. \tag{13}$$

The solution of this subproblem solved in L-C domain is identified on the basis function described in Eq.(13) and the set of parameters (A,B,b_k,θ_k).

2.1.4. LCT inversion method for sinusoidal functions

In LCT inversion method for sinusoidal functions proposed in Hun et al. (2023), the authors defined the solution f of the problem in time t as a sine series such that :

$$f(t) = \sum_{k=1}^{N} a_k \sin(\omega_k t + \phi_k), \tag{14}$$

with the set $\mathbf{A_k} = (a_k,\omega_k,\phi_k)$ of parameters to be identified, which are respectively the amplitude, the pulsation and the shift of the approached function. The analogous form in L-C domain of this projection basis is defined as :

$$f^{\star}(p) = \sum_{k=1}^{N} \left\{ a_k \frac{p^2}{\omega_k^2 + p^2} \sin(\phi_k) + a_k \frac{\omega_k p}{\omega_k^2 + p^2} \cos(\phi_k) \right\}. \tag{15}$$

The solution function $f^{\star}$ is then estimated on several discrete points p_i and an algorithm allows the identification of the set $\mathbf{A_k}$ and the reconstruction in the time domain.

2.2. Time homogenization for VEVP material

2.2.1. General problem

For the mechanical problem with VEVP material the evolution equations in time t are written as follows :

- Field equations :

$$\mathcal{P}(t) = \begin{cases} \boldsymbol{\varepsilon}(\mathbf{x},t) = \boldsymbol{\varepsilon}^{ve}(\mathbf{x},t) + \boldsymbol{\varepsilon}^{vp}(\mathbf{x},t), \\ \boldsymbol{\sigma}(\mathbf{x},t) = \displaystyle\int_{-\infty}^{t} \mathbb{C}(\mathbf{x},t-\psi) : \dot{\varepsilon}^{ve}(\mathbf{x},\psi) d\psi, \\ \nabla \cdot \boldsymbol{\sigma}(\mathbf{x},t) + \rho \mathbf{F}(\mathbf{x},t) = \mathbf{0}, \\ f(\sigma(\mathbf{x},t), R(\mathbf{x},t)) = \sigma_{eq}(\mathbf{x},t) - \sigma_y(\dot{\epsilon}(\mathbf{x},t)) - R(p(\mathbf{x},t)), \\ \dot{\epsilon}^{vp}(\mathbf{x},t) = \boldsymbol{B}(\sigma(\mathbf{x},t), p(\mathbf{x},t)), \\ \dot{p}(\mathbf{x},t) = C(\sigma(\mathbf{x},t), p(\mathbf{x},t)), \end{cases} \tag{16}$$

where the following notation is introduced :

- $\varepsilon^{ve}, \varepsilon^{vp}$ are the viscoelastic and viscoplastic strain tensors
- $\mathbb{C}(t)$ is the fourth-order isotropic relaxation tensor as described in Eq.(2), the stress-strain relation can be written as :

$$\boldsymbol{\sigma}(t) = \mathbb{C}_{\infty} : \boldsymbol{\epsilon}^{ve}(t) + \sum_{i=1}^{I} \boldsymbol{s}_i(t) + \sum_{j=1}^{J} \sigma_{Hj}(t)\mathbf{1}, \tag{17}$$

with $\mathbb{C}_{\infty} = 3K_{\infty}\mathbb{I}^{vol} + 2G_{\infty}\mathbb{I}^{dev}$ the long-term elastic Hooke's operator and :

$$\begin{cases} \boldsymbol{s}_i(t) = 2G_i \exp\left(-\dfrac{t}{g_i}\right) \displaystyle\int_{-\infty}^{t} \exp\left(\frac{\eta}{g_i}\right) \frac{\partial \boldsymbol{\xi}^{ve}(\eta)}{\partial \eta} d\eta \\ \sigma_{Hj}(t) = 3K_j \exp\left(-\dfrac{t}{k_j}\right) \displaystyle\int_{-\infty}^{t} \exp\left(\frac{\eta}{k_j}\right) \frac{\partial \varepsilon_H^{ve}(\eta)}{\partial \eta} d\eta \end{cases} \tag{18}$$

$\boldsymbol{\xi}$(t) is the deviatoric tensor and ε_H(t) the dilatational part of the strain tensor.

- f is the Von Mises yield surface, where

$$\begin{cases} \sigma_{eq} = \left(\frac{3}{2}\boldsymbol{s} : \boldsymbol{s}\right)^{\frac{1}{2}} \text{ is the Von Mises stress,} \\ \qquad \boldsymbol{s} = \boldsymbol{\sigma} - \frac{1}{3} tr(\boldsymbol{\sigma})\mathbf{1} \text{ is deviatoric part of Cauchy stress,} \\ \sigma_y \text{ is the initial yield stress,} \\ R(p) \text{ is a hardening function,} \end{cases} \tag{19}$$

- $\boldsymbol{B}(t) = \dot{p}\boldsymbol{N}$ gives the VP strain evolution, with $\boldsymbol{N} = \frac{3}{2}\frac{s}{\sigma_{eq}}$

- $C(t)$ is a VP function

The constitutive models for $R(p)$ and $C(t)$ will be identify and numercially simulated in Section 3.

- Boundary conditions :

$$\mathcal{B}(t) : \begin{cases} \partial\Omega_u \cap \partial\Omega_T = \varnothing, \ \partial\Omega_u \cup \partial\Omega_T = \partial\Omega, \\ u_i(\mathbf{x}, t) = u_i^d(\mathbf{x}, t), \text{ on } \partial\Omega_u, \\ T_i(\mathbf{x}, t) = T_i^d(\mathbf{x}, t), \text{ on } \partial\Omega_T, \end{cases} \tag{20}$$

2.2.2. Computational method

In order to accelerate the computational time to access to a local solution, a time homogenization procedure has been proposed by Haouala and Doghri (2015). In this work, the physical time t has been described on two time scales : macro-scale $\bar{t}$ and micro-scale τ, as shown in Fig. 5 and mathematically defined as :

$$t = \bar{t} + T\tau, \text{ with } \bar{t} \in [0, T_M] \text{ and } \tau \in [0, 1], \tag{21}$$

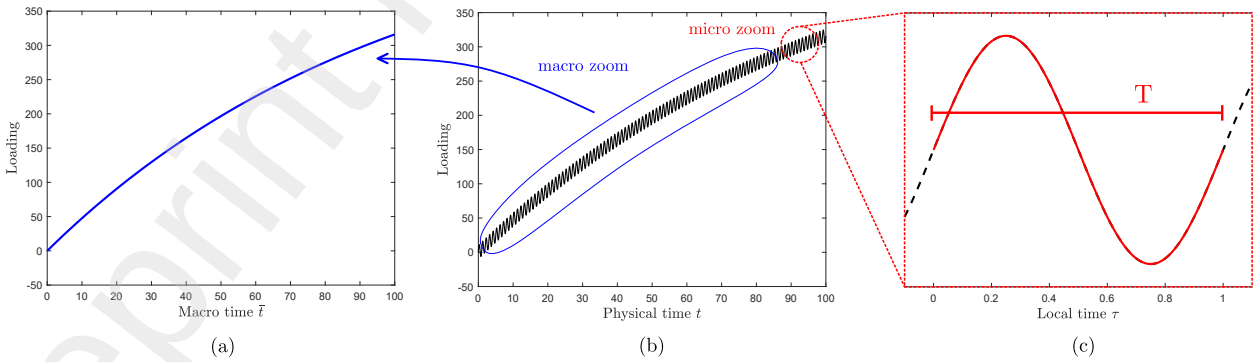

Figure 5: Macro and micro time coordinates ($\bar{t}$: macro time, t : physical time, τ micro-time)

With this time description, the response fields $\Phi(\mathbf{x}, t)$ defined classically at a given spatial location $\mathbf{x} \in \Omega$ and in physical time t can be expressed as field functions ϕ depending on the two time scales $\bar{t}$ and τ expressed as :

$$\Phi(\mathbf{x}, t) = \phi(\mathbf{x}, \bar{t}, \tau) \tag{22}$$

This time description of the response fields has been then decomposed into two parts : a macroscopic field $\bar{\phi}$ and an oscillatory field $\widetilde{\phi}$ written as :

$$\phi(\mathbf{x}, \bar{t}, \tau) = \bar{\phi}(\mathbf{x}, \bar{t}) + \widetilde{\phi}(\mathbf{x}, \bar{t}, \tau), \tag{23}$$

the macroscopic part $\bar{\phi}$ is the average value of the function ϕ with the respect to the fast time scale τ and the macro time $\bar{t}$ described as follows :

$$\bar{\phi}(\mathbf{x}, \bar{t}) = \int_0^1 \phi(\mathbf{x}, \bar{t}, \tau) d\tau \tag{24}$$

With this time description, the problem can be written as :

$$\mathcal{P}(\bar{t}, \tau) : \begin{cases} \boldsymbol{\varepsilon}(\mathbf{x}, \bar{t}, \tau) = \boldsymbol{\varepsilon}^{ve}(\mathbf{x}, \bar{t}, \tau) + \boldsymbol{\varepsilon}^{vp}(\mathbf{x}, \bar{t}, \tau), \\ \boldsymbol{\sigma}(\mathbf{x}, \bar{t}, \tau) = \mathbb{C}_\infty : \boldsymbol{\epsilon}^{ve}(\mathbf{x}, \bar{t}, \tau) + \sum_{i=1}^{I} \boldsymbol{s}_i(\mathbf{x}, \bar{t}, \tau) + \sum_{j=1}^{J} \sigma_{Hj}(\mathbf{x}, \bar{t}, \tau)\mathbf{1}, \\ \nabla \cdot \boldsymbol{\sigma}(\mathbf{x}, \bar{t}, \tau) + \mathbf{f}(\mathbf{x}, \bar{t}, \tau) = \mathbf{0}, \\ f(\sigma(\mathbf{x}, \bar{t}, \tau), R(\mathbf{x}, \bar{t}, \tau)) = \sigma_{eq}(\mathbf{x}, \bar{t}, \tau) - \sigma_y(\dot{\epsilon}(\mathbf{x}, \bar{t}, \tau)) - R(p(\mathbf{x}, \bar{t}, \tau)), \\ \dot{\epsilon}^{vp}(\mathbf{x}, \bar{t}, \tau) = \boldsymbol{B}(\sigma(\mathbf{x}, \bar{t}, \tau), p(\mathbf{x}, \bar{t}, \tau)), \\ \dot{p}(\mathbf{x}, \bar{t}, \tau) = C(\sigma(\mathbf{x}, \bar{t}, \tau), p(\mathbf{x}, \bar{t}, \tau)), \end{cases} \tag{25}$$

and

$$\mathcal{B}(\bar{t}, \tau) : \begin{cases} \partial\Omega_u \cap \partial\Omega_T = \varnothing, \ \partial\Omega_u \cup \partial\Omega_T = \partial\Omega, \\ u_i(\mathbf{x}, \bar{t}, \tau) = u_i^d(\mathbf{x}, \bar{t}, \tau), \text{ on } \partial\Omega_u, \\ T_i(\mathbf{x}, \bar{t}, \tau) = T_i^d(\mathbf{x}, \bar{t}, \tau), \text{ on } \partial\Omega_T, \end{cases} \tag{26}$$

Under the assumptions of the regularity of the fields ϕ, T-periodicity and for a long time evolution T_F ($\frac{T}{T_F} \ll 1$, T_F is the final time), an asymptotic series of power of T on the fields ϕ can be employed as follows :

$$\phi(\bar{t}, \tau) = \sum_{i=0}^{\infty} T^i \phi_i(\bar{t}, \tau), \tag{27}$$

the field ϕ can be regarded as consisting of a leading term ϕ_0 and a series of rapidly decreasing amplitude terms as

$$\phi(\mathbf{x}, \bar{t}, \tau) \simeq \phi_0(\mathbf{x}, \bar{t}, \tau) + T\phi_1(\mathbf{x}, \bar{t}, \tau) + \dots . \tag{28}$$

In this procedure, the asymptotic expansions applied on the associated fields are injected into the equations of the problem (Eqs. (16) and (26)). Gathering terms of equal order, the problem has been rewritten in terms of the powers of T. Finally, taking the average of all zero-order equations, a decomposition of the problem in so-called macro-chronological problem and micro-chronological problem, according to the split of Eq.(23) is obtained. It is shown in Haouala and Doghri (2015) that for each macro-time $\bar{t}$, first one solves a purely VE problem in the micro-time τ. Next, a VEVP problem (with the VE part known) is solved in the macro-time $\bar{t}$ completed by the following initial conditions :

$$\bar{\mathbf{u}}_0(\mathbf{x}, \bar{t}=0) + \widetilde{\mathbf{u}}_0(\mathbf{x}, \bar{t}=0, \tau=0) = \mathbf{u}^{\mathbf{I}}(\mathbf{x}), \text{ in } \boldsymbol{\Omega} \tag{29}$$

$$\bar{\boldsymbol{\sigma}}_0(\mathbf{x}, \bar{t}=0) + \widetilde{\boldsymbol{\sigma}}_0(\mathbf{x}, \bar{t}=0, \tau=0) = \boldsymbol{\sigma}^{I}(\mathbf{x}), \text{ in } \Omega \tag{30}$$

The numerical implementation details, and the excellent accuracy of this method are reported in Haouala and Doghri (2015). In practice, that work developed the time homogenization method only for one volume element assuming the total strain history is known and actually, solids and structures were not simulated. This issue will be adressed in the present article.

3. Model parameter identification procedures

The methodology developed in this paper is applied to lattice structures, more specifically, TPU polymer structures printed with the selective laser sintering (SLS) process, as described in Cobian et al. (2022). The SLS process introduces micro porosity on the fabricated parts, accounting for up to 5% of the overall volume (Lucarini et al. (2022)).
In order to apply our procedure, we started by identifying the polymer matrix properties without porosity from experimental measurements. Secondly, the identified properties were employed to describe the behaviors of both matrix and weak spots microscale description. The model parameter identification procedures used in each step will be presented in the following two subsections.

3.1. Characterization of TPU matrix properties without porosity

Two main experimental measurements were performed to identify TPU matrix properties:

- Dynamic mechanical analysis (DMA),
- Uniaxial tensile tests at different strain rates.

It should be mentioned that the VE properties were identified independently from VP ones. Therefore, we used first DMA experimental measurements to determine the set of VE model parameters:

$$\Theta^{VE} = (G_0, K_0, \nu, G_i, g_i, K_j, k_j), \text{ with } i \in [1, I], j \in [1, J] \tag{31}$$

where (G_0, K_0) are the instantaneous shear and bulk moduli, ν is the Poisson's ratio, (G_i, K_j) are the shear and bulk relaxation moduli of the Prony series defined in Eqs.(3) and (4), respectively. (g_i, k_j) represent respectively,the shear and bulk relaxation times. I and J are the number of Prony series branches.

Secondly, we used the pre-determined VE properties in addition to the uniaxial tensile loading measurements, at different strain rates $\dot{\varepsilon}_{1\mapsto 3}$, to identify the VP model parameters :

$$\Theta^{VP} = (\sigma_y, (k_1, k_2, n), (\eta, m)) \tag{32}$$

where σ_y is the initial yield stress, (k_1, k_2, n) are the isotropic hardening model parameters following :

$$R(p) = k_1 p + k_2(1 - \exp(-np)) \tag{33}$$

and (η, m) are VP function parameters following :

$$C(t) = g_v(f) = \frac{\sigma_y}{\eta}\left(\frac{f}{\sigma_y + R(p)}\right)^m, \text{ if } f > 0;\ g_v = 0, \text{ if } f \leq 0 \tag{34}$$

The model parameter identification was performed using Digimat MX module (Digimat software by Hexagon). The latter module was coupled with a VE-VP mean field homogenization (MFH) code based on the incremental secant method Haddad et al. (2022) in order to account for porosity within the tested specimens. In fact, MFH code was used to predict the effective behavior of porous TPU matrix incorporating a known set of model parameters. Then Digimat MX is employed to minimize the discrepancy between experimental measurements and MFH predictions by adjusting both Θ^{VE} and Θ^{VP} set of parameters.

3.1.1. Identification of TPU VE properties

Dynamic Mechanical Thermal Analysis (DMTA) was performed with an Eplexor 500 N (Netzsch-Gerätebau GmbH, Selb, Germany) in the test temperature range from -80 °C to 100 °C. The test cycles started at the lowest temperature and the values were increased in increment of 10 K. The test frequency was varied for all temperatures from 0.5 up to 50 Hz. The dynamic wave amplitude was a sine wave with mean strain levels of 15% (TPUs) and dynamic peak-to-peak (p-p) amplitudes of 2% (TPUs). The parameter-set was selected to characterize the materials within the linear viscoelastic regime. In order to compensate the thermal elongation, a holding force of 0.5 N was set, and the initial length at isothermal conditions was measured. At each testing temperature, pre-cycles under the same conditions as those mentioned above were performed for 1 s to avoid stress softening effects. The geometry of the used specimen is depicted in Fig.6.

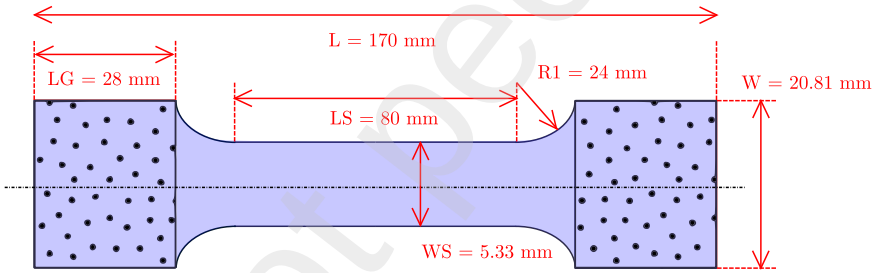

Figure 6: Geomerty of the dumbbell specimen used for DMA test in addition to uniaxial tension experiments under different strain rates.

During the DMA, the specimens were subjected to sinusoidal displacement such that the total strain is :

$$\varepsilon(t) = \varepsilon_0 \sin(\omega\, t) \tag{35}$$

where ε_0 and ω are the imposed amplitude and frequency, respectively. The specimens response is expressed hereafter:

$$\sigma(t) = \sigma_0 \sin(\omega\, t + \delta) \tag{36}$$

with σ_0 representing the stress magnitude and δ the delay between the applied load and the response.

Using Eqs. (35) and (36), a relaxation modulus $E(t)$ in the frequency domain can be deduced as follows :

$$E(t) = \frac{\sigma(t)}{\varepsilon(t)} \longrightarrow E^*(i\omega) = \frac{\sigma_0}{\varepsilon_0} \exp(i\delta) = E^{*'}(\omega) + iE^{*''}(\omega) \tag{37}$$

The assumed VE model follows a generalized Maxwell model. The latter implies that the relaxation modulus is written using Prony series as in Eqs.(3) and (4).

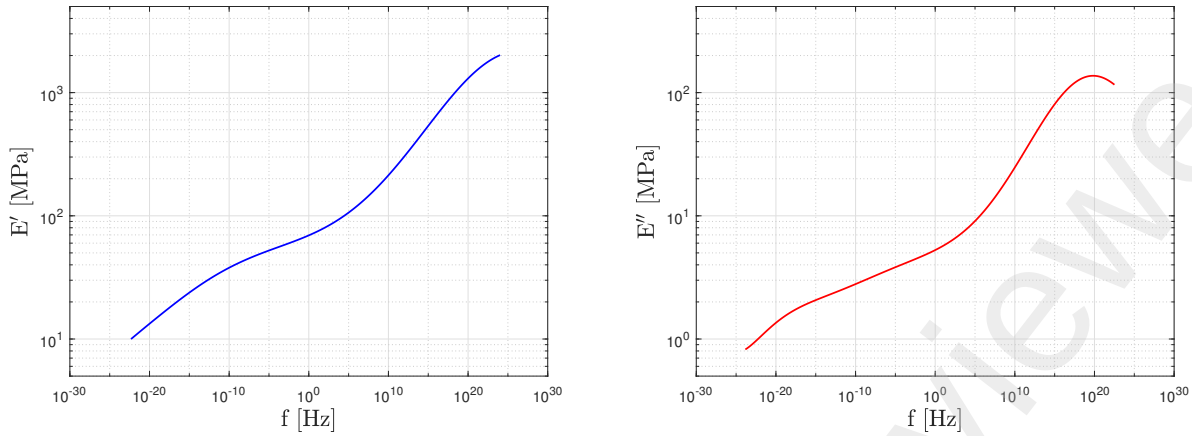

Figure 7: Time-Temperature superposition master curves for storage modulus E' and loss modulus E'' values.

Therefore, in the frequency domain, the relaxation modulus $E(t)$ is recast as:

$$E^*(i\,\omega) = E_\infty + \sum_{i=1}^{I} E_i \frac{\omega^2}{\left(\frac{1}{\tau_i}\right)^2 + \omega^2} + i \sum_{i=1}^{J} E_i \frac{\frac{\omega}{\tau_i}}{\left(\frac{1}{\tau_i}\right)^2 + \omega^2} \tag{38}$$

Where E_∞ and E_i are the long-term and instantaneous relaxation moduli, τ_i represents the relaxation times, I and J designate the number of shear and bulk relaxation moduli respectively.
Consequently, both storage and loss moduli can be written as:

$$E^{*'}(\omega) = E_\infty + \sum_{i=1}^{I} E_i \frac{\omega^2}{\left(\frac{1}{\tau_i}\right)^2 + \omega^2} \tag{39}$$

$$E^{*''}(\omega) = \sum_{i=1}^{J} E_i \frac{\frac{\omega}{\tau_i}}{\left(\frac{1}{\tau_i}\right)^2 + \omega^2} \tag{40}$$

The latter two equations express the evolution of the storage and loss moduli in the frequency domain. They were used by Digimat MX to fit the master curves deduced from Fig. 7 . We should mention that the frequency range chosen to identify the VE properties corresponds to strain rates from $[10^{-6}$ - $10^{3}]\mathrm{s}^{-1}$. It appears also that $I = J = 3$ shear and bulk relaxation moduli were sufficient to fit the VE part of the TPU behavior.

3.1.2. Identification of TPU VP properties

Monotonic uniaxial tensile tests were conducted at different test rates $\dot{\varepsilon}_{1\mapsto 3}$ (0.1, 1, 10 s^{-1}) using a high rate servohydraulic testing machine (MTS Damper Test System) and force-displacement curves were measured. The measurements were included in Digimat MX in addition to the pre-determined VE properties Θ^{VE} (from Section 3.1.1) in order the retrieve

the VP model parameters Θ^{VP}. The software minimizes the mean square error between VP part of experimental results and the effective responses of the porous TPU matrix predicted using the homogenization code.

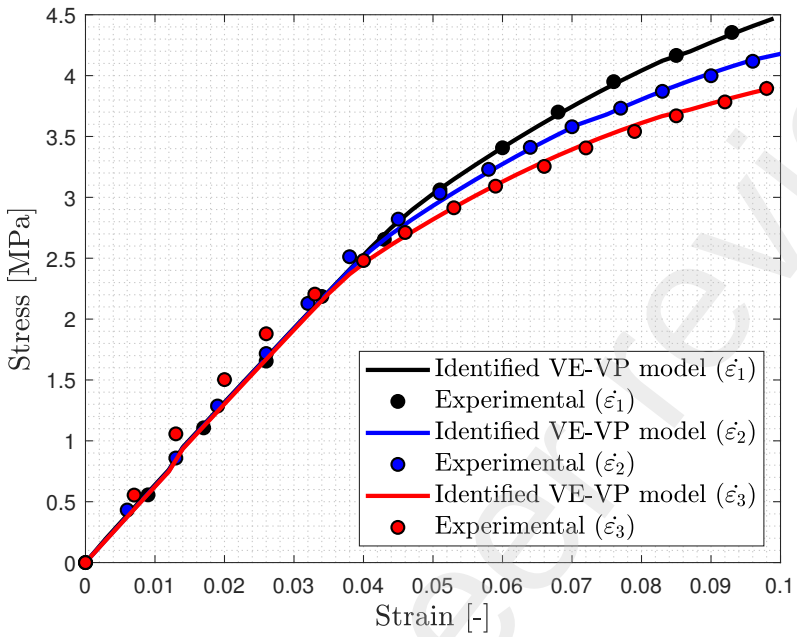

Figure 8: Comparison between experimental measurements and the identified homogenized VEVP model, specimen with TPU material printed using SLS process at 20°C.

3.1.3. Identification of VEVP homogenized properties

The identification of VEVP model is complex with $N(\Theta^{VEVP}) = 19$ parameters. For this purpose, a first identification has been made based on experimental DMA tests, fixing the elastic and $N(\Theta^{VE}) = 14$ VE parameters. For the other $N(\Theta^{VP}) = 5$ parameters, the traction tests at different strain rates are used and minimizing the mean square error with the simulations. After fixing the yield stress $\sigma_y = 2.0$ MPa, a full optimization has been performed on the same traction test, adjusting all the VEVP parameters Θ^{VEVP}. The comparison of the identified VEVP parameters and the experimental traction test for different strain rate is depicted in Fig.8 and the VEVP homogenized parameters are reported in Table 1.

4. Reference solution and verification of hybrid method for N = 100 cycles

In this part, the structure considered is a unit cell of a 3D TPU lattice, see Figure. 9, under a cyclic torsion loading $T_d^{(1)} = (-T_d, 0, 0)$, $T_d^{(2)} = (0, 0, -T_d)$, $T_d^{(3)} = (T_d, 0, 0)$, $T_d^{(4)} = (0, 0, T_d)$, where $T_d = T_d(t)$ is the sum of Heavyside and periodic time functions described in Eqs. (9) to (11). T_d is parameterized with $|T_d| = 50$ N and ($\hat{A} = 1$ N , $\hat{\theta} = 0.01$ s^{-1} , $\tilde{A} = 0.1$ N ,$\tilde{\omega} = 12.7$ rad.s^{-1}). The VEVP reference solution computed in time (Eq. (16)) uses the VE an VP parameter sets Θ^{VE} and Θ^{VP} explicited in Table 1. The FE solver uses an implicit dynamic time scheme algorithm. The structure is submitted to a loading for N-cycles ($t \in [0; 50]$s, $\Delta t = 0.005$s, $N_c \sim 100$ cycles). The VE $(\mathcal{P}, \mathcal{B})$ problem is solved by using the LCT and the

Elastic parameters Θ^E	Initial Young's modulus [MPa]	Poisson's ratio [ ]
	$E_0 = 88.7$	$\nu_0 = 0.3$

VE parameters Θ^{VE}	Prony series	
Shear	modulus G_i [MPa]	relaxation times g_i [s]
	3.42	1.55×10^{-2}
	3.08	1.59×10^{-3}
	4.26	1.64×10^{-4}
Compressibility	modulus K_j [MPa]	relaxation times k_j [s]
	7.42	7.14×10^{-3}
	6.68	7.35×10^{-4}
	9.24	7.56×10^{-5}

VP parameters Θ^{VP}	modulus [MPa]	exponent [ ]
Initial yield stress	$\sigma_y = 2.00$	
Isotropic hardening	$(k_1/k_2) = (1.0/1.0)$	$n = 1370$
Viscoplastic function	$\eta = 4.96.10^3$	$m = 11.97$

Table 1: Parameters (Θ^{VE},Θ^{VP}) of homogenized VEVP specimen with TPU material printed by SLS additive manufacturing process at 20°C.

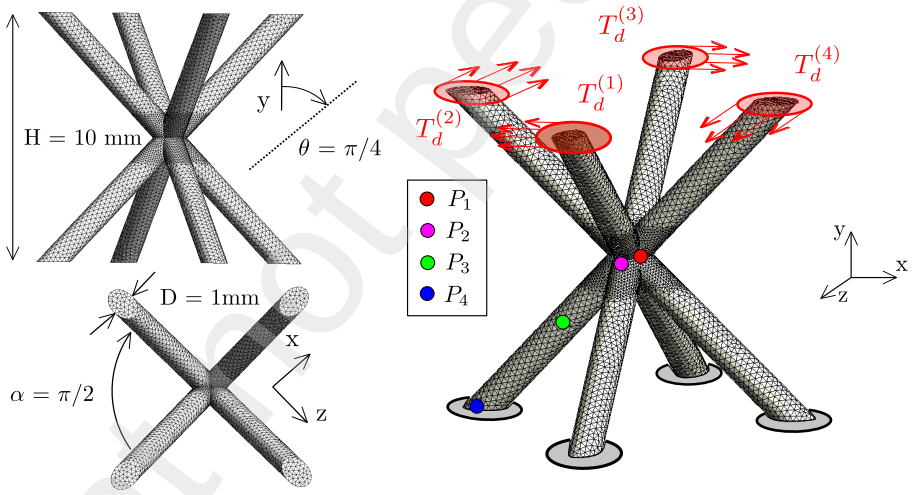

Figure 9: Unit cell of a 3D TPU Lattice : geometry, boundary conditions and P_i Gauss points of interest.

inverse LCT procedure described in Section 2.1 and summarized in Fig. 4; it is parameterized only by the set of VE parameters Θ^{VE} referenced in first part of Table 1. The hybrid solution is built by the VE strain solution and the VEVP time-homogenization of Section 2.2, using the material parameters of Table 1. The investigation based on the comparison of the 3 problems (reference VEVP, VE, Hybrid) will be shown hereafter.

Figure 10 compares the strain component histories between the VEVP reference and the VE simulations at the 4 Gauss points of interest.
Figure 11 shows the comparison of stress component histories between the VEVP reference and the proposed hybrid method.

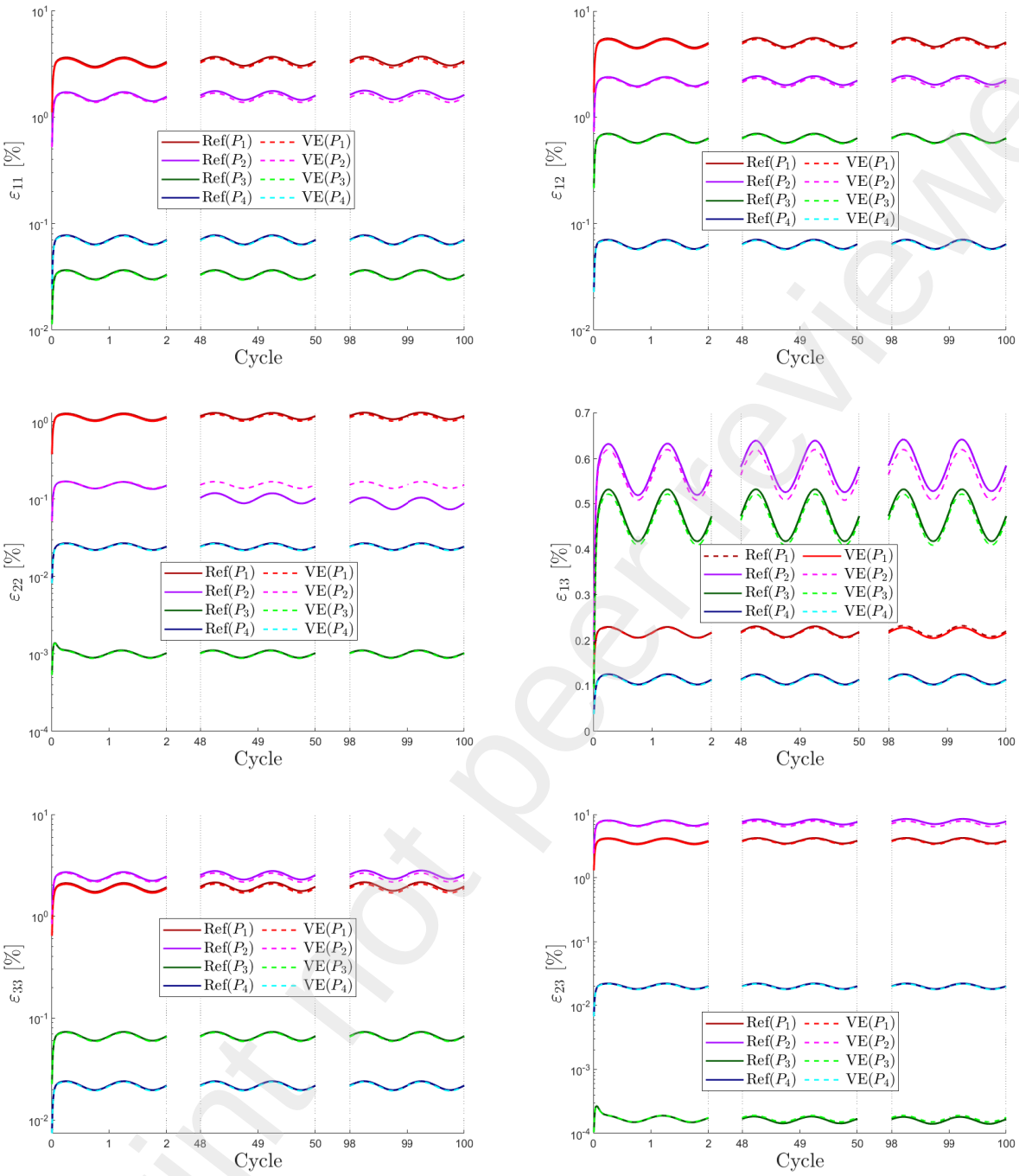

Figure 10: Unit cell of 3D lattice under N = 100 loading cycles. Comparison of the absolute values of ε_{ij} strain components at 4 points of interest of Figure. 9, between the VEVP reference solution and VE solution obtained by LCT and inverse LCT procedure.

Figure 10 enables to validate the hypothesis linking the reference VEVP and the VE solutions, which is that is both analyses lead approximately to the same total strain histories regardless of the space location of the material points. Consequently, the VE strain history will be used as input to the VEVP time-homogenization method in the proposed hybrid formulation.

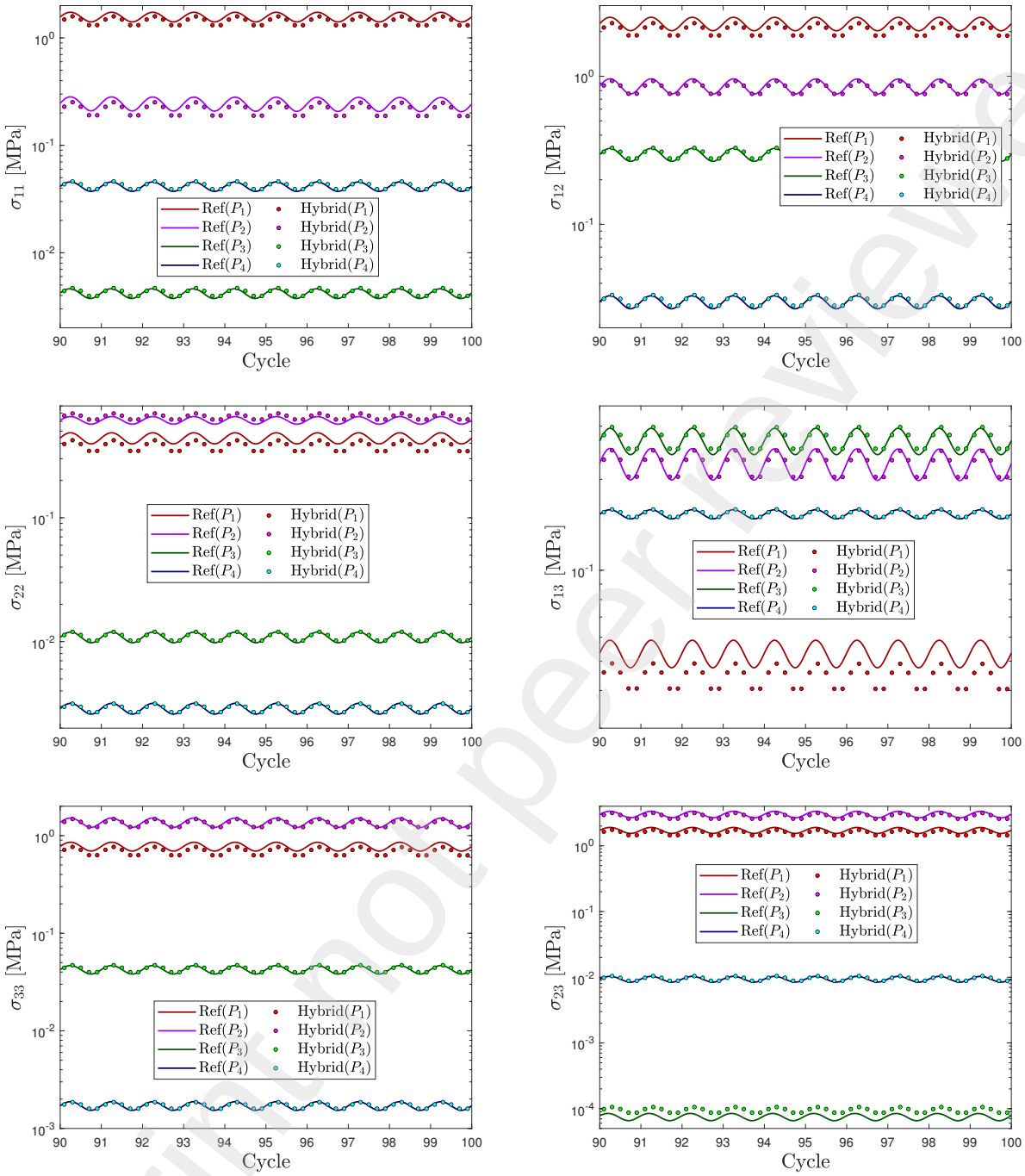

Figure 11: Unit cell of 3D lattice under N = 100 loading cycles. Comparison of the absolute values of σ_{ij} stress components at 4 points of interest of Figure. 9, computed with VEVP reference solution and the proposed hybrid (VE strain + VEVP time-homogenization) solution.

Figure. 11 shows the stress histories between the reference solution (VEVP full calculation) and the hybrid solution (using the time-homogenization method) in the 10 last cycles. The error between all these responses are slight.

In Figure. 12, a local energy indicator defined on the finite element volume V_e as :

$$W(\boldsymbol{x},t) = \int_{Ve} \sigma(\boldsymbol{x},t) : \varepsilon(\boldsymbol{x},t) dV \tag{41}$$

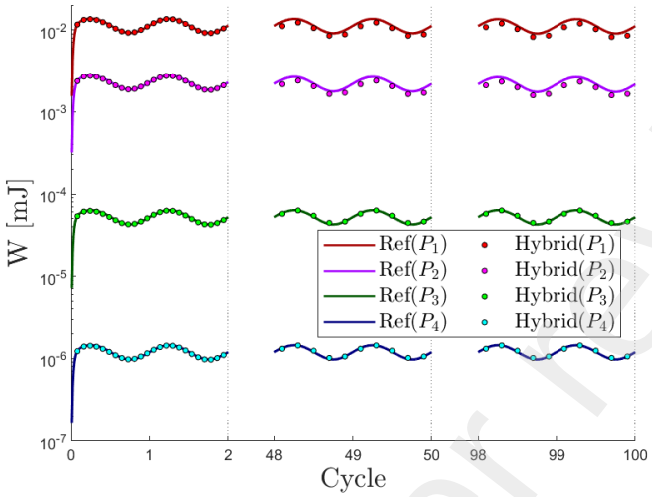

Figure 12: Unit cell of 3D lattice N = 100 loading cycles. Comparison of energy indicator at 4 points of interest of Figure. 9, computed with VEVP reference solution, and hybrid (VE strain + VEVP time-homogenization) solution.

and based on the total strain and total stress is computed for the reference and the hybrid method. It can be observed that the energy indicators for each method match well.

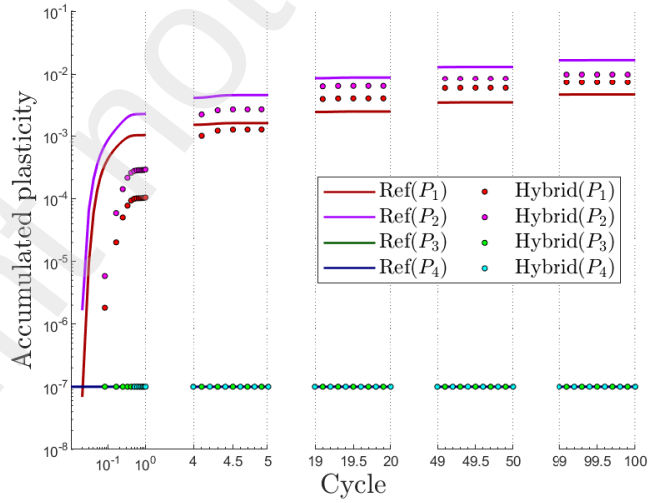

Figure 13: Unit cell of 3D lattice under N = 100 loading cycles. Comparison of accumulated plastic strain p at 4 points of interest of Figure 9, computed with VEVP reference solution, and hybrid (VE strain + VEVP time-homogenization) solution.

Figure 13 compares the accumulated plasticity between the reference and the hybrid solution at the 4 Gauss points

Figure. 13 shows that the plasticity occurs in the center of the structure, indicated by the points P_1,P_2. The accumulated plasticity values computed by the hybrid and reference methods show a slight difference. However, the hybrid method is based on the time-homogenization formulation which is valid for a large number of cycles while the comparison between hybrid and the reference solutions is limited to $N = 100$ cycles, which is the computational hardware limit of our VEVP reference simulations.

5. Predictions with hybrid method for N = 1M loading cycles

The hybrid method is efficient for a large number of cycles, an application for N = 1 million cycles and various predictions are shown hereafter. For the strain and stress, two scalar metrics are used. For the strain, we define the equivalent strain as :

$$\varepsilon^{eq} = \sqrt{\frac{3}{2}(e_{11}^2 + e_{22}^2 + e_{33}^2) + 3(\varepsilon_{12}^2 + \varepsilon_{13}^2 + \varepsilon_{23}^2)}, \tag{42}$$

with e_{ii} the components of the deviatoric strain tensor.

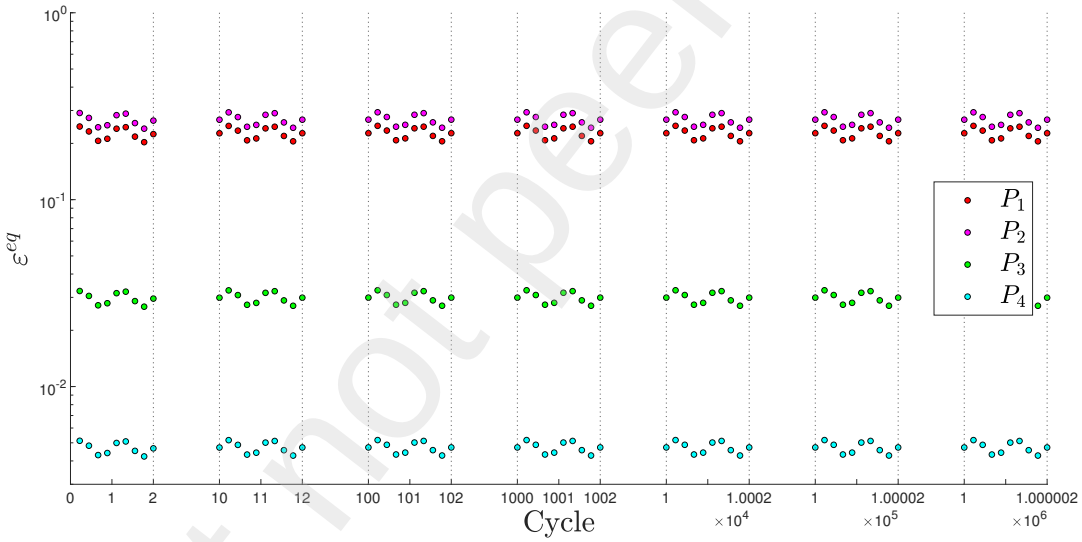

Figure 14: Unit cell of 3D lattice under N = 1M cycles. Predictions of equivalent strain with proposed hybrid method at 4 points of interest.

For the stress, the metric used is the von-Mises stress defined as :

$$\sigma^{VM} = \sqrt{\frac{1}{2}((\sigma_{11} - \sigma_{22})^2 + (\sigma_{22} - \sigma_{33})^2 + (\sigma_{33} - \sigma_{11})^2) + 3(\sigma_{12}^2 + \sigma_{13}^2 + \sigma_{23}^2)} \tag{43}$$

Figures 14 and 15, show the evolution of the strain and stress metrics for N = 1M cycles. Predictions at points P_3 and P_4 fluctuate over all the cycles, by staying in the VE domain. For points P_1 and P_2, the predictions of the von-Mises stress σ^{VM} are still decreasing at N = 1M cycles, showing that this region continues to plastify, after a large number of cycles. This slow evolution is captured by the hybrid method.

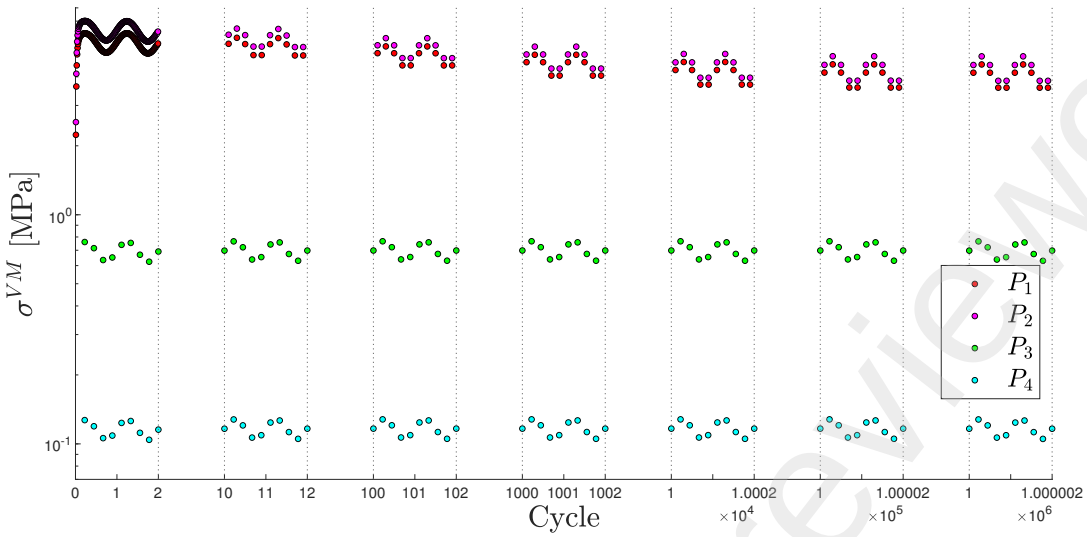

Figure 15: Unit cell of 3D lattice under N = 1M cycles. Predictions of von-Mises equivalent stress with proposed hybrid method at 4 points of interest.

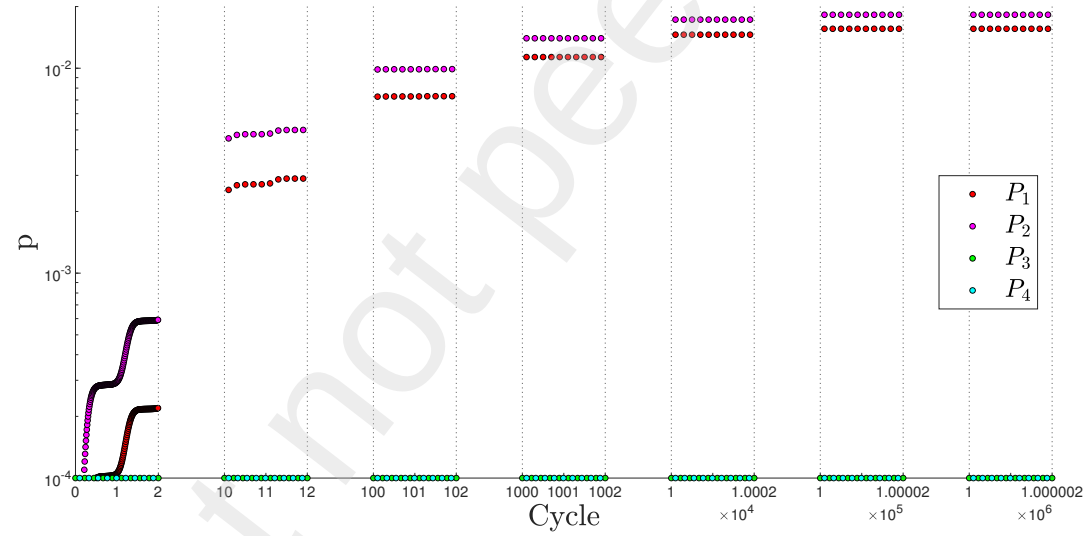

Figure 16: Unit cell of 3D lattice under N = 1M cycles. Predictions of accumulated plastic strain with proposed hybrid method at 4 points of interest.

Figure. 16 shows the accumulated plasticity. As mentionned for the strain and stress observation, points P_1, P_2 continue to plastify compared to the points P_3, P_4. The solution presented in this section cannot be obtained by a classical full VEVP analysis, because the computational cost for N = 1M cycles would be too prohibitive, as explained in Section 6.

6. Comparison of computational costs

In this part, the numerical costs of the full reference VEVP calculation, the VE method (LCT + inverse LCT) and the hybrid solution (based on VE total strains histories and VEVP time-homogenization) are provided. The study shows the performance of each method and was

applied on N = 100 and N = 1M cycles. It should be noted that the reference and the VE solutions are provided for the entire structure, whereas with the hybrid solution only for the 4 local points of interest ($P_{1\mapsto 4}$). As for the solution tools, reference VEVP solutions in time are provided by CM3 code (C/C++) CM3 (2024), with parallel architecture and developed in ULiège. The computation has been performed using 6 CPU. The VE and hybrid solutions used ABAQUS (2009) for the computation on LC domain and MATLAB Inc. (2022) for the inversion in time, the time homogenization and the post-processing using only 1CPU. The computational information between the Reference, VE and hybrid methods are reported in Table 2. The computational time used is provided for N = 100 cycles and N = 1M cycles. More precise details, described for each step of simulation are provided in Appendix A, Table A.3

Method	Reference solution	VE solution	hybrid solution
Software Architecture/Ressource	python/C++ (CM3) parallel/6 CPU	Abaqus/matlab 1CPU	Abaqus/matlab 1CPU
Solution strain history stress history Accumulated plasticity	Structural Computed Computed Computed	Structural Computed Computed N/A	Local (4 Gauss points) Provided (input) Computed Computed
time N = 100 cycles time N = 1M cycles	17.5 hours 20.5 years	21.5 hours 21.5 hours	5 minutes 32 hours

Table 2: Computational details and time simulation for 3 methods : Reference VEVP, VE, and hybrid method.

7. Conclusions

In this paper, a new computational time reduction method for solving VEVP polymer structural problems under large number of loading cycles was proposed. This so-called hybrid method is based on two key pillars, described in Section. 2. The first is based on LCT and inverse LCT and enables to recover the VE structural solution. The second pillar is based on time-homogenization and allows to recover the stress and plastic strain solutions at local points. Both methods have shown a great time performance for a very large number of cycles. The main idea was to couple them by assuming the same strain history between VE and VEVP calculations.

Before the numerical investigation, an experimental study, described in Section. 3 has been conducted to identify the VEVP properties of the TPU polymer material printed by SLS process. The identification is based on DMA and traction tests with different strain rates. The VEVP parameters are then inferred as an input for numerical study to investigate the accuracy of the hybrid method. The VE properties are the VE part of the VEVP model.

The numerical investigation started with different comparisons. In Section 4, a simulation on a 3D lattice subjected to cyclic torsion, has been performed for $N = 100$ cycles (our computational hardware limit to access the reference solution). The study, for different points of the 3D structure, is focused on comparing : strain/stress components, accumulated plasticity and energy between the solutions of the VEVP reference, the VE and hybrid methods. The hypothesis of the equivalence between the VE and reference strain histories

has been verified, validating the hybrid method and the link between the VE structural solution using Laplace-Carson transform and the time-homogenization method. For this number of cycles, limited by hardware resource used to access the reference solution, the study shows that for the local points, far from plasticity area, the hybrid, VE and reference results match well. In critical zone, with the highest von-Mises stress, the same comparison has been performed and demonstrates the accuracy of the hybrid solution with respect to the reference. It should be noted that the hybrid method can capture the accumulated plasticity. In Section 5 the hybrid method was used to simulate the 3D lattice for N = 1 million cycles. The evolutions of strain, stress and the accumulated plasticity have been captured on this much larger range of cycles.

Concerning the computational time used for N = 1 million cycles, the access to the reference solution over all the structure, using parallel architecture and 6 CPUs, can be estimated to 20 years. For the hybrid technique and for a restricted numbers of points of interest (4 in this study), the access to the complete VEVP solution uses 35 hours and 1 CPU.

The low computational cost of the hybrid method proposed in the present article opens naturally the way to the multiscale prediction of high cycle fatigue life for polymer solid and structures. THis is an ongoing work which will be reported in a future publication.

Declaration of competing interest

The authors declare that they have no known competing financial interests or personal relationships that could have appeared to influence the work reported in this paper.

Acknowledgments

The present work was conducted and funded within the framework of the European Union's Horizon 2020 research and innovation programme for the project "Multi-scale Optimisation for Additive Manufacturing of fatigue resistant shock-absorbing MetaMaterials (MOAMMM)", grant agreement No. 862015, of the H2020-EU.1.2.1. - FET OpenProgramme.

Data availability

The data used in this work can be downloaded on the git : https://gitlab.uliege.be/moammm

References

ABAQUS, 2009. Michael Smith. Dassault Systèmes Simulia Corp, United States.

Bahloul, A., Doghri, I., Adam, L., 2021. Linking a phase field model for polymer crystallization to full-field micromechanical simulations of semi-crystalline polymers. Computational Materials Science 199, 110685. doi:https://doi.org/10.1016/j.commatsci.2021.110685.

Bahloul, A., Doghri, I., Adam, L., 2023. Mesoscale modelling of polymer powder densification due to thermal sintering. Applied Mathematical Modelling 114, 408–422. doi:https://doi.org/10.1016/j.apm.2022.09.022.

Balieu, R., Lauro, F., Bennani, B., Delille, R., Matsumoto, T., Mottola, E., 2013. A fully coupled elastoviscoplastic damage model at finite strains for mineral filled semi-crystalline polymer. International Journal of plasticity 51, 241–270. doi:https://doi.org/10.1016/j.ijplas.2013.05.002.

Bird, R.B., Carreau, P.J., 1968. A nonlinear viscoelastic model for polymer solutions and melts—i. Chemical Engineering Science 23, 427–434. doi:https://doi.org/10.1016/0009-2509(68)87018-6.

Bottasso, C.L., 2002. Multiscale temporal integration. Computer Methods in Applied Mechanics and Engineering 191, 2815–2830. doi:https://doi.org/10.1016/S0045-7825(02)00219-0.

CM3, 2024. CM3 Finite Element Solver for Multiphysics Problems. Computational and Multiscale Mechanics of Materials laboratory, ULiège, Belgium. URL: https://gitlab.onelab.info/cm3/cm3Libraries.git.

Cobian, L., Rueda-Ruiz, M., Fernandez-Blazquez, J., Martinez, V., Galvez, F., Karayagiz, F., Lück, T., Segurado, J., Monclus, M., 2022. Micromechanical characterization of the material response in a pa12-sls fabricated lattice structure and its correlation with bulk behavior. Polymer Testing 110, 107556. URL: https://www.sciencedirect.com/science/article/pii/S0142941822000812, doi:https://doi.org/10.1016/j.polymertesting.2022.107556.

Cognard, J.Y., Ladevèze, P., 1993. A large time increment approach for cyclic viscoplasticity. International Journal of plasticity 9, 141–157. doi:https://doi.org/10.1016/0749-6419(93)90026-M.

Desmorat, R., Kane, A., Seyedi, M., Sermage, J.P., 2007. Two scale damage model and related numerical issues for thermo-mechanical high cycle fatigue. European Journal of Mechanics-A/Solids 26, 909–935. doi:https://doi.org/10.1016/j.euromechsol.2007.01.002.

Findley, W.N., Lai, J.S., Onaran, K., 1989. Creep and relaxation of nonlinear viscoelastic materials - With an introduction to Linear Viscoelasticity. Dover Publications, New York.

Frank, G.J., Brockman, R.A., 2001. A viscoelastic–viscoplastic constitutive model for glassy polymers. International Journal of Solids and Structures 38, 5149–5164. doi:https://doi.org/10.1016/S0020-7683(00)00339-5.

Gravouil, A., Combescure, A., 2001. Multi-time-step explicit–implicit method for non-linear structural dynamics. International Journal for Numerical Methods in Engineering 50, 199–225. doi:https://doi.org/10.1002/1097-0207(20010110)50:1<199::AID-NME132>3.0.CO;2-A.

Guennouni, T., 1988. Sur une méthode de calcul de structures soumises à des chargements cycliques: l'homogénéisation en temps. ESAIM: Mathematical Modelling and Numerical Analysis 22, 417–455.

Haddad, M., Doghri, I., Pierard, O., 2022. Viscoelastic-viscoplastic polymer composites: Development and evaluation of two very dissimilar mean-field homogenization models. International Journal of Solids and Structures 236-237, 111354. URL: https://www.sciencedirect.com/science/article/pii/S0020768321004273, doi:https://doi.org/10.1016/j.ijsolstr.2021.111354.

Haouala, S., Doghri, I., 2015. Modeling and algorithms for two-scale time homogenization of viscoelastic-viscoplastic solids under large numbers of cycles. International Journal of Plasticity 70, 98–125. doi:https://doi.org/10.1016/j.ijplas.2015.03.005.

Hasan, O., Boyce, M., 1995. A constitutive model for the nonlinear viscoelastic viscoplastic behavior of glassy polymers. Polymer Engineering & Science 35, 331–344. doi:https://doi.org/10.1002/pen.760350407.

Heczko, J., Kottner, R., 2018. Modeling of material damage using finite elements and time homogenization in case of finite strain. Applied Mathematics and Computation 319, 264–273. doi:https://doi.org/10.1016/j.amc.2017.03.014.

Hughes, T.J., Stewart, J.R., 1996. A space-time formulation for multiscale phenomena. Journal of computational and applied mathematics 74, 217–229. doi:https://doi.org/10.1016/0377-0427(96)00025-8.

Hun, D.A., Haddad, M., Doghri, I., 2023. Modeling and simulation of viscoelastic solids under large numbers of loading cycles. Mechanics of Advanced Materials and Structures 30, 1542–1558. doi:https://doi.org/10.1080/15376494.2022.2037170.

Inc., T.M., 2022. MATLAB. The MathWorks Inc., Natick, Massachusetts, United States. URL: https://www.mathworks.com.

Jegou, L., Marco, Y., Le Saux, V., Calloch, S., 2013. Fast prediction of the wöhler curve from heat build-up measurements on short fiber reinforced plastic. International Journal of fatigue 47, 259–267. doi:https://doi.org/10.1007/s00161-017-0561-2.

Johnsen, J., Clausen, A.H., Grytten, F., Benallal, A., Hopperstad, O.S., 2019. A thermo-elasto-viscoplastic constitutive model for polymers. Journal of the Mechanics and Physics of Solids 124, 681–701. doi:https://doi.org/10.1016/j.jmps.2018.11.018.

Krairi, A., Doghri, I., 2014. A thermodynamically-based constitutive model for thermoplastic polymers coupling viscoelasticity, viscoplasticity and ductile damage. International Journal of Plasticity 60, 163–181. doi:https://doi.org/10.1016/j.ijplas.2014.04.010.

Krairi, A., Doghri, I., Robert, G., 2016. Multiscale high cycle fatigue models for neat and short fiber reinforced thermoplastic polymers. International Journal of Fatigue 92, 179–192. doi:https://doi.org/10.1016/j.ijfatigue.2016.06.029.

Kujawski, D., Ellyin, F., 1995. A unified approach to mean stress effect on fatigue threshold conditions. International Journal of Fatigue 17, 101–106. doi:https://doi.org/10.1016/0142-1123(95)95888-N.

Launay, A., Maitournam, M., Marco, Y., Raoult, I., 2013. Multiaxial fatigue models for short glass fibre reinforced polyamide. part ii: Fatigue life estimation. International Journal of Fatigue 47, 390–406. doi:https://doi.org/10.1016/j.ijfatigue.2012.09.015.

Lucarini, S., Cobian, L., Voitus, A., Segurado, J., 2022. Adaptation and validation of fft methods for homogenization of lattice based materials. Computer Methods in Applied Mechanics and Engineering 388, 114223. URL: https://www.sciencedirect.com/science/article/pii/S0045782521005545, doi:https://doi.org/10.1016/j.cma.2021.114223.

Magri, M., Lucarini, S., Lemoine, G., Adam, L., Segurado, J., 2021. An fft framework for simulating non-local ductile failure in heterogeneous materials. Computer Methods in Applied Mechanics and Engineering 380, 113759. doi:https://doi.org/10.1016/j.cma.2021.113759.

Mallick, P., Zhou, Y., 2004. Effect of mean stress on the stress-controlled fatigue of a short e-glass fiber reinforced polyamide-6, 6. International journal of fatigue 26, 941–946. doi:https://doi.org/10.1016/j.ijfatigue.2004.02.003.

Mandel, J., 1966/re-edited 1994, J. Gabay. Cours de mécanique des milieux continus. volume I and II. Gauthier-Villars.

Meneghetti, G., Ricotta, M., Lucchetta, G., Carmignato, S., 2014. An hysteresis energy-based synthesis of fully reversed axial fatigue behaviour of different polypropylene composites. Composites Part B: Engineering 65, 17–25. doi:https://doi.org/10.1016/j.compositesb.2014.01.027.

Meraghni, F., Nouri, H., Bourgeois, N., Czarnota, C., Lory, P., 2011. Parameters identification of fatigue damage model for short glass fiber reinforced polyamide (pa6-gf30) using digital image correlation. Procedia Engineering 10, 2110–2116. doi:https://doi.org/10.1016/j.proeng.2011.04.349.

Miled, B., Doghri, I., Delannay, L., 2011. Coupled viscoelastic–viscoplastic modeling of homogeneous and isotropic polymers: Numerical algorithm and analytical solutions. Computer methods in applied mechanics and engineering 200, 3381–3394. doi:https://doi.org/10.1016/j.cma.2011.08.015.

Mortazavian, S., Fatemi, A., 2017. Fatigue of short fiber thermoplastic composites: A review of recent experimental results and analysis. International Journal of Fatigue 102, 171–183. doi:https://doi.org/10.1016/j.ijfatigue.2017.01.037.

Oskay, C., Fish, J., 2004. do. International Journal for Numerical Methods in Engineering 61, 329–359. doi:https://doi.org/10.1002/nme.1069.

Raphael, I., Saintier, N., Rolland, H., Robert, G., Laiarinandrasana, L., 2019. A mixed strain rate and energy based fatigue criterion for short fiber reinforced thermoplastics. International Journal of Fatigue 127, 131–143. doi:https://doi.org/10.1016/j.ijfatigue.2019.06.003.

Santharam, P., Marco, Y., Le Saux, V., Le Saux, M., Robert, G., Raoult, I., Guévenoux, C., Taveau, D., Charrier, P., 2020. Fatigue criteria for short fiber-reinforced thermoplastic validated over various fiber orientations, load ratios and environmental conditions. International Journal of Fatigue 135, 105574. doi:https://doi.org/10.1016/j.ijfatigue.2020.105574.

Schapery, R., 1965. A method of viscoelastic stress analysis using elastic solutions. Journal of the Franklin Institute 279, 268–289. doi:10.1016/0016-0032(65)90339-X.

Shaw, M.T., MacKnight, W.J., 2018. Introduction to polymer viscoelasticity. John Wiley & Sons.

Tao, G., Xia, Z., 2007. Ratcheting behavior of an epoxy polymer and its effect on fatigue life. Polymer testing 26, 451–460. doi:https://doi.org/10.1016/j.polymertesting.2006.12.010.

Uchida, M., Tada, N., 2013. Micro-, meso-to macroscopic modeling of deformation behavior of semi-crystalline polymer. International Journal of Plasticity 49, 164–184. doi:https://doi.org/10.1016/j.ijplas.2013.03.007.

Van Dommelen, J.v., Parks, D., Boyce, M., Brekelmans, W., Baaijens, F., 2003. Micromechanical modeling of the elasto-viscoplastic behavior of semi-crystalline polymers. Journal of the Mechanics and Physics of Solids 51, 519–541. doi:https://doi.org/10.1016/S0022-5096(02)00063-7.

Wang, S., Tang, S., He, C., Wang, Q., 2023. Cyclic deformation and fatigue failure mechanisms of thermoplastic polyurethane in high cycle fatigue. Polymers 15, 899. doi:https://doi.org/10.3390/polym15040899.

Wu, L., Kilingar, N.G., Noels, L., et al., 2020. A recurrent neural network-accelerated multi-scale model for elasto-plastic heterogeneous materials subjected to random cyclic and non-proportional loading paths. Computer Methods in Applied Mechanics and Engineering 369, 113234. doi:https://doi.org/10.1016/j.cma.2020.113234.

Zaïri, F., Naït-Abdelaziz, M., Gloaguen, J.M., Lefebvre, J.M., 2008. Modelling of the elasto-viscoplastic damage behaviour of glassy polymers. International Journal of Plasticity 24, 945–965. doi:https://doi.org/10.1016/j.ijplas.2007.08.001.

Appendix A. Computational time comparison TO READ OR TO CANCEL !

Reference structure	- Number of cycles dependence - $N = 100$	Final time $\sim$ 17.5 h
VEVP solver :	6 CPU, Parallel computing, CM3(C/C++)	Total time $\sim$ 17.5 h
Time domain		Cumulative time = 63k s
	time for one cycle	time = 630 s
	time for $N_c = 100$ cycles	time = time x 100
VE structure solution	- Number of cycle independance - $N = \infty$	Final time $<$ 21 h
Elastic (linear) solver :	1 CPU, Abaqus	Total time $\sim$ 4 min
L-C domain		Cumulative time = 228 s
	time for one discrete p_i point	time = 3.80 s
	for $N_{p_i} = 30$ discrete points	time = time x 30
	for 2 boundary displacement functions	time = time x 2
LCT inversion :	1 CPU, Matlab	Total time $<$ 20.3h
Schapery's collocation method		Cumulative time = 5 h
	Calculation	time = 0.027 s
	for $N_e(\sim 55k)$ element	time = time x 55k
	for components of fields $(\boldsymbol{\varepsilon}, \boldsymbol{\sigma})$	time = time x 12
LCT inversion for sinusoidal function		Cumulative time $<$ 15.3 h
	Calculation	time = 0.083 s
	for $N_e(\sim 55k)$ elements	time = time x 55k
	for components of fields $(\boldsymbol{\varepsilon}, \boldsymbol{\sigma})$	time = 12 x time
hybrid local solution	- Number of cycle independance - $N = 100$	Final time $<$ 5 min
Elastic (linear) solver :	1 CPU, Abaqus	Total time $\sim$ 4 min
L-C domain		Cumulative time = 228 s
	time for one discrete p_i point	time = 3.80 s
	for $N_{p_i} = 30$ discrete points	time = time x 30
	for 2 boundary displacement functions	time = time x 2
LCT inversion :	1 CPU, Matlab	Total time = 3s
Schapery's collocation method		Cumulative time = 0.7s
	Calculation	time = 0.027 s
	for $N_e = 4$ elements	time = time x 4
	for components of fields $(\boldsymbol{\varepsilon})$	time = time x 12
LCT inversion for sinusoidal function		Cumulative time = 2 s
	Calculation	time = 0.083 s
	for $N_e = 4$ elements	time = time x 4
	for components of fields $(\boldsymbol{\varepsilon})$	time = 2 x time
Time homogenization :	1 CPU, Matlab	Total time = 11.5s
Schapery's collocation method		Cumulative time = 11.5s
	Calculation for 1 cycle	time = 0.0048 s
	for $N_c = 100$ cycles	time = time x 100
	for $N_e = 4$ elements	time = time x 4
	for components of fields $(\boldsymbol{\sigma})$	time = time x 6

Table A.3: Computational time details.

Declaration of interests

☐ The authors declare that they have no known competing financial interests or personal relationships that could have appeared to influence the work reported in this paper.

☒ The authors declare the following financial interests/personal relationships which may be considered as potential competing interests:

Hun Darith Anthony reports financial support was provided by MOAMMM project. Hun Darith Anthony reports a relationship with MOAMMM project that includes: employment. If there are other authors, they declare that they have no known competing financial interests or personal relationships that could have appeared to influence the work reported in this paper.